communications physics

Article

https://doi.org/10.1038/s42005-024-01862-9

Time persistence of climate and carbon flux networks

Check for updates

Ting Qing [1,2,3], Fan Wang[2,4], Qiuyue Li[2], Gaogao Dong [1,5] ✉, Lixin Tian [1,6,7,8,9] ✉ & Shlomo Havlin [2] ✉

The persistence of the global climate system is critical for assuring the sustainability of the natural ecosystem. However, persistence at a network level has been rarely discussed. Here we develop a framework to analyze the time persistence of the yearly networks of climate and carbon flux, based on cross-correlations between sites, using daily data from China, the contiguous United States, and the Europe land region. Our framework for determining the persistence is based on analyzing the similarity between the network structures in different years. Our results reveal that the similarity of climate and carbon flux networks in different years are within the range of 0.57 ± 0.07, implying that the climate and carbon flux in the Earth's climate system are generally persistent and in a steady state. We find a very small decay in similarity when the gap between years increases. Moreover, we find that the persistence of climate variables and carbon flux in the three regions decreases when considering only long range links. Analyzing the persistence and evolution of the climate and carbon flux networks, enhance our understanding of the spatial and temporal evolution of the global climate system.

The Earth's climate system is a persistent and stable complex system in which all climate variables interact, and this persistence has a crucial impact on the health and sustainability of the ecological environment and species diversity[1–3]. With the increasing human activities and modern technology, a significant amount of greenhouse gases, including carbon dioxide, is emitted into the Earth's atmosphere through massive burning of fossil fuels, industrial processes, and changes in land use, which is one of the important factors leading to global climate change[4]. The sustainable development of ecosystems and socioeconomic advancement depend largely on the persistence of the Earth's climate system. Therefore, a deeper understanding of the persistence of climate variables, which evolve over time, is crucial for understanding, predicting, and responding to climate warming. Furthermore, the persistence of the Earth's climate system during climate change has not been studied systematically.

There exist many studies on the time persistence of dynamics represented by single nodes, e.g., climate variables at a given location[5,6], or brain signals[7], that characterize the persistence of a variable at a certain location. However, persistence at a network level, i.e., the persistence of the topology of the network links, has been rarely discussed. In recent years, the study of time persistence of local temporal events has attracted researchers from different fields[1], such as the field of geophysics[8] and the field of atmospheric oceans[9], since many related temporal phenomena (rainfall, wind, temperature, etc.) are at a given location inherently persistent and nor randomly independent. Here, we develop a framework to study the time persistence of a climate network, and we apply it to climate and carbon flux systems. Our framework for determining the persistence is based on analyzing the similarity between the climate networks, i.e., the network links, in different years based on the Jaccard index. The question of the persistence of the climate network as a whole can lead to in-depth insight into the climate mechanisms, help to improve climate models, and test if and how global warming affects this global persistence synchronization.

The primary climatic variables, including temperature, wind speed, precipitation, and geopotential height, have a significant impact on climate change in the Earth system. Wunderling et al.[10] used a network model of four interacting climate tipping elements to investigate in different temperature scenarios, the effect of climate change. Meanwhile, based on the potential teleconnections among the tipping elements, researchers systematically studied the impact of the Amazon Rainforest Area on global

[1]School of Mathematical Sciences, Jiangsu University, Zhenjiang, 212013 Jiangsu, China. [2]Department of Physics, Bar-Ilan University, Ramat-Gan, 52900, Israel. [3]Data Recovery Key Laboratory of Sichuan Province, College of Mathematics and Information Science, Neijiang Normal University, Neijiang, 641100, China. [4]School of Mathematical Sciences, Nanjing Normal University, Nanjing, 210023, China. [5]School of Emergency Management, Jiangsu University, Zhenjiang, 212013 Jiangsu, China. [6]Research Institute of Carbon Neutralization Development, School of Mathematical Sciences, Jiangsu University, Zhenjiang, 212013, China. [7]Jiangsu Province Engineering Research Center of Industrial Carbon System Analysis, School of Mathematical Sciences, Jiangsu University, Zhenjiang, 212013, China. [8]Jiangsu Province Engineering Research Center of Spatial Big Data, School of Mathematical Sciences, Nanjing Normal University, Nanjing, 210023, China. [9]Key Laboratory for NSLSCS, Ministry of Education, School of Mathematical Sciences, Nanjing Normal University, Nanjing, 210023, China. ✉e-mail: gago999@126.com; tianlx@ujs.edu.cn; havlins@gmail.com

climate change using the global near-surface air temperature field[11]. With the increase in human activities, there has been a significant change not only in the global surface temperature but also in the sea surface temperature, which has a wide-range impact on the global climate system. Systematic studies of trends, variability, and persistence of sea surface temperature enable the analysis of the mechanisms and patterns of climate change, and thus contributing to obtain a better understanding of climate change processes[12]. Persistent extreme heat events under the influence of global climate change have severe impacts on ecosystems and societies. Rousi et al.[13] identified Europe as a heatwave hotspot and found that its upward trend in heatwave occurrence over the last 42 years was related to atmospheric dynamics induced by an increase in the frequency and persistence of double jets over the Eurasian continent. Wind speed, as a crucial climatic variable, directly influences atmospheric and oceanic circulation, thereby affecting the global climate system. Koçak et al.[14] based on autocorrelation function, conditional probabilities, and wind speed duration curves methods, analyzed wind speed data in northwestern Turkey. Their results indicate that the proposed methods clearly reflect the persistence properties of the wind speed in the studied area. In addition, the climate system is a complex and giant system[15], and its properties and phenomena can be analyzed and better understood from a network perspective using sophisticated methods of network science[16]. In this approach, regions are viewed as nodes and correlations between climate variables of pairs of nodes are considered as links[17], providing a new perspective for understanding the Earth's climate system. Numerous studies have explored climate networks. For instance, constructing climate networks based on extreme winter precipitation in the United States enabled the identification of regions of extreme precipitation and the climatic conditions that lead to extreme precipitation[18]. We note that climate variables have been used to study the critical thresholds of climate change and provide early warning signals[19–22]. Moreover, integrating climate network methods have been applied to identify and measure the optimal paths that yield the interaction between pairs of remote nodes, i.e., teleconnections[23]. Furthermore, climate networks are known to generally present significant correlations when they are geographically close; while the correlations between sites at far distances are largely influenced by external and global atmospheric processes. For example, it is found the origin of a significant correlation between remote nodes is due to their correlations with atmospheric Rossby waves[24,25]. These studies provide a crucial scientific basis and methods to deepen our understanding of the mechanisms and patterns behind climate change.

In 2014, the Intergovernmental Panel on Climate Change (IPCC)'s Fifth Scientific Assessment Report concluded that the global average temperature of land and ocean surfaces increased by 0.85 [0.65-1.06]°C from 1880 to 2012, mainly due to the significant increase in the concentration of carbon dioxide in the atmosphere[26]. While the terrestrial ecosystem and the oceanic system can effectively remove CO_2 from the atmosphere, the carbon flux can reflect whether, at a given moment in time, a region is a carbon source area (emitting more CO_2 than it absorbs) or a carbon sink area (removing more CO_2 than it emits). If man-made emission sources (i.e., carbon sources) exceed the natural removal processes, it will inevitably lead to a rise in atmospheric CO_2 concentrations. Therefore, in addition to studying climate variables such as temperature and precipitation, it is crucial to also study carbon flux to understand changes in the Earth's climate system and the effects of global warming.

Overall, investigating the persistence of carbon flux and climate variables networks is essential for maintaining the stability of the Earth's climate system which requires significant attention. The present persistence study uses climate variables (temperature, wind speed, precipitation, and potential height) and carbon flux data in the Earth's climate system for the past 20 years. By combining network analysis of climate variables and carbon flux, we construct the corresponding complex network systems of climate and carbon flux, and other variables to investigate the persistence of the network structure of the climate system from spatial and temporal perspectives during the past 20 years. With our developed model, one can observe the persistence of climate and carbon flux network structure during the past 20 years, by using the Jaccard index. In addition, we explored the persistence of climate and carbon flux networks at different spatial distances. The results show a decreasing trend of persistence with increasing spatial distance.

Methods

Network inference

Here, we select three important geographical regions that have had a significant impact on global development in the past 20 years: East Asia (China (CHN)), the Americas (the Contiguous United States (USA)), and Europe (EU). The study is based on the daily average datasets of climate variables (temperature, wind speed, precipitation, and geopotential height)[27] and carbon flux[28] in the three aforementioned regions. The datasets are evenly distributed and interpolated into $2^{\circ} \times 2^{\circ}$ grids, generating total of $N_A = 238$ (CHN), 200 (USA), and 385 (EU) grid points. For more details, see Supplementary Notes 1 (SN1).

The datasets of both carbon flux and climate variables contain strong nonlinear trends and seasonal signals. Hence, to mitigate the effects of trends, the data has been preprocessed following Ref. 22. To this end, we set $\widehat{C}_i(t')(i = 1, 2, \ldots, N_A, t' = 1, 2, \ldots, \widehat{L})$, $\widehat{G}_i(t')\,(i = 1, 2, \ldots, N_A, t' = 1, 2, \ldots, \widehat{L})$, $\widehat{T}_i(t')(i = 1, 2, \ldots, N_A, t' = 1, 2, \ldots, \widehat{L})$, $\widehat{W}_i(t')\,(i = 1, 2, \ldots, N_A, t' = 1, 2, \ldots, \widehat{L})$, $\widehat{P}_i(t')(i = 1, 2, \ldots, N_A, t' = 1, 2, \ldots, \widehat{L})$ as the original time series of carbon flux, geopotential height, temperature, wind speed and precipitation at grid point i, respectively. Here N_A is the number of nodes and $\widehat{L} = 365 \times 20$ (days) (February 29 has been removed). We removed the strong seasonal trends by de-trending the original data. We achieved this by subtracting the corresponding centered 30-day "moving" averages from the time series of each variable, and normalizing it by the standard deviation of these 30 days[29,30]. This process helps to reduce the trends and noise impacts which is useful for evaluating the underlying cross-correlations representing the strength of the links. According to the above steps, the carbon flux, geopotential height, temperature, wind speed, and precipitation time series for each grid point are obtained and expressed respectively as $C_i(t')$, $G_i(t')$, $T_i(t')$, $W_i(t')$, and $P_i(t')$.

Next, we consider the grid sites as the nodes of the network, and the cross-correlations between the time series of different pairs of the grid sites are regarded as the links of the network. Using network science methods[17], we study the cross-correlations within the same climatic variables, thereby measuring the interactions and relations between different locations.

The correlation pattern, i.e., the network structure of the system, evolves with time, and to avoid losing important information, we apply the sliding window method by dividing the entire time series into smaller fragments. By doing so, we can obtain at each sliding window the climate network that captures the system's evolving correlation pattern. One advantage of using the sliding window method is that the sliding window has the properties of memory and transitivity, which are important in studying the correlation patterns of a system over time[31]. With the above method, the time series of climate variables for each pair of grid points can be potentially linked to construct the interaction network. Only significant links where their signal-to-noise ratio is high ($p < 0.1$) are considered significant links when constructing the climate network. The evolution of this network could reveal systematically the complexity and the spatio-temporal characteristics of the climate system. Specifically, for the data of carbon flux and climate variables, we construct a time-series network with a sliding window of L ($L = 365 \times 2 + 90$ days), where the moving step is set to 365 days. Thus the time series of climate and carbon flux are divided into 18 segments of length L (due to the 365 days overlap). Within the t-th window, we compute the correlation matrix $X(t)$, in which the element $X_{i,j}$ is the cross-correlation representing the links that connect node i and node j. First, the time-delayed cross-correlation function between the two-time series $Y_i(t)$ and $Y_j(t)$ is calculated, see refs. 23,25,32–34,

$$X_{i,j}(\tau) = \frac{\langle Y_i(t)Y_j(t+\tau)\rangle - \langle Y_i(t)\rangle\langle Y_j(t+\tau)\rangle}{\sigma_{Y_i(t)}\sigma_{Y_j(t+\tau)}}, \quad (1)$$

where $\langle Y_i(t)\rangle$ and $\sigma_{Y_i(t)}$ represent the average and standard deviation of $Y_i(t)$, respectively. $\tau \in [-\tau_{max}, \tau_{max}]$ is the time lag, with $\tau_{max} = 90$ days. The choice of τ_{max} helps to ensure a reliable estimation of the seasonal noise level in the cross-correlation. According to the time inversion symmetry, we can obtain $X^t_{i,j}(-\tau) = X^t_{j,i}(\tau)$[35]. We identify the value of the highest peak of the absolute value of the cross-correlation function and denote the corresponding time lag of this peak to be τ^*. The correlation between node i and node j is thus $X_{i,j} = X_{i,j}(\tau^*)$. The direction of the link $X_{i,j}(\tau^*)$ is from i to j when $\tau^* > 0$ and from j to i when $\tau^* < 0$. The direction is undefined when $\tau^* = 0$. Within each window, we quantify the strength or weight of the links (correlations) using[17,36]:

$$w_{i,j} = \frac{X_{i,j}(\tau^*) - \overline{X_{i,j}(\tau)}}{\sigma_{X_{i,j}(\tau)}}, \quad (2)$$

where $\overline{X_{i,j}(\tau)}$, $\sigma_{X_{i,j}(\tau)}$ represent the mean and standard deviation over all τ values of the cross-correlation function, respectively. Based on the above steps, we construct a series of time-dependent climate and carbon flux networks. A demonstration of 2017–2018 carbon flux data in the USA as an example to establish the links, is shown in Fig. 1. In Fig. 1b and c, one can see that the peak point of the correlation coefficient of its links corresponds to $\tau^* = 1$, which implies that the time delay between these locations of carbon flux is 1 day from west to east.

Significant tests

In this study, a shuffling procedure is used to test the statistical significance of the calculated link weights. The significance test is as follows. For each pair of climate variables denoted by nodes i and node j, for node i, we use the sequence of the t-th time window, and for node j, we use a sequence taken from a randomly chosen time window, which we call shuffled, where we repeated the shuffling process 50 times. Subsequently, the significant links are determined by comparing their actual correlation value to the shuffled correlation coefficients. In this shuffling approach, we preserve the distribution of values and the natural auto-correlations in each year for each shuffled record. If the original link strength (cross-correlation value) significantly exceeds those of the shuffled control, we identify it as a real link; otherwise, it is regarded as a spurious link. Due to the distinct characteristics of positive weighted ($w^+_{i,j}$) and negative weighted ($w^-_{i,j}$) (of positive correlations and negative correlations, respectively), critical threshold $\theta_+(\theta_-)$ is set to be such that a correlation value is regarded to be real when it has a probability below 1% to be random, i.e., $p < 0.01$. In Fig. 2, the dashed lines represent the location of the thresholds where the real cross-correlations values appear to have a probability of at least 100 times higher than that of random. Thus, we obtain the weighted adjacency matrix $W(t)$ of the climate variables links in the t-th time window. For instance, we illustrate the probability distribution function of link weights for the original and shuffled data for the 2017–2018 time window in Fig. 2. It is seen from Fig. 2 that the threshold appears to be mostly for W above a value close to 4, that is, above this value of W, the probability of a link being false diminishes to less than 1%. Note that the fraction of links as a function of the threshold also supports the reliability of this threshold since only above this threshold does the fraction of links highly increase (see SN2 Fig. S17). Note also, that $W = 4$ means that the peak value of the shifted cross-correlation function is above 4 standard deviations from all correlation values (For $W = 4$ as the threshold, the variation in the fraction of significant links with year is shown in SN2 Fig. S18). Note that similar results are seen for other years, see SN2 Figs. S2–S16.

In addition, we analyze the probability distribution functions of time lags of the links between different locations for the studied climate variables and carbon flux, as shown in Fig. 3 (similar results of wind speed and precipitation, are shown in SN2 Fig. S19). It can be seen that the maximum value of the time lags of most climate variables and carbon flux is 0, 1, or −1, i.e., $\tau^* = 0$, 1, or −1 day. This indicates that the time delay between most locations of climate variables and carbon flux is within 1 day from west to east (The number and fraction of significant links between west to east and east to west at a time lag $\tau^* = \pm 1$ are shown in SN2 Supplementary Tables I–IX). The size of these time lags and the direction of the network structure may be related to atmospheric circulation patterns, ocean surface temperature distribution, and other climatic phenomena. For increasing geographical distance (as shown in SN2 Figs. S20 and S21), the time lag increases, but the maximum value does not exceed 1 or −1.

Next, we investigate the relationship between correlation strength and distance. The geographical distance is calculated based on the latitude and longitude coordinates of the two nodes. Since the geographic distance dataset is discrete, we divide its range into uniform intervals of 200 km, which is approximately the distance between neighboring nodes. This partitioning enables us to assign each pair of nodes to a specific interval according to their geographic distance, denoted as $dis_{i,j} \in (dis_n, dis_{n+1}]$. Here, $dis_{i,j}$ denotes the geographic distance between node i and node j, and dis_n and dis_{n+1} represent the n-th and $(n+1)$-th distance intervals, respectively. Figure 4 shows the fraction of significant links of climate and carbon flux with respect to their geographic distance in the different time series of $dis \in (dis_n, dis_{n+1}]$ (similar results of wind speed and precipitation, are shown in SN2 Fig. S22). These findings suggest that, in general, nodes closer in proximity exhibit a higher number of significant links. This is expected since winds or other transport processes move the climate and carbon between nearby locations, and the further the places are, the similarity between locations, which is represented by links, becomes weaker. However, strong outliers are also observed. In many cases, there is a bump of many long-range links for distances of a few thousand kilometers. This indicates that the mechanism is dominated not by transportation, e.g., due to winds, but by the potential influence of an external player on both locations, such as the Rossby waves, which have similar patterns in different

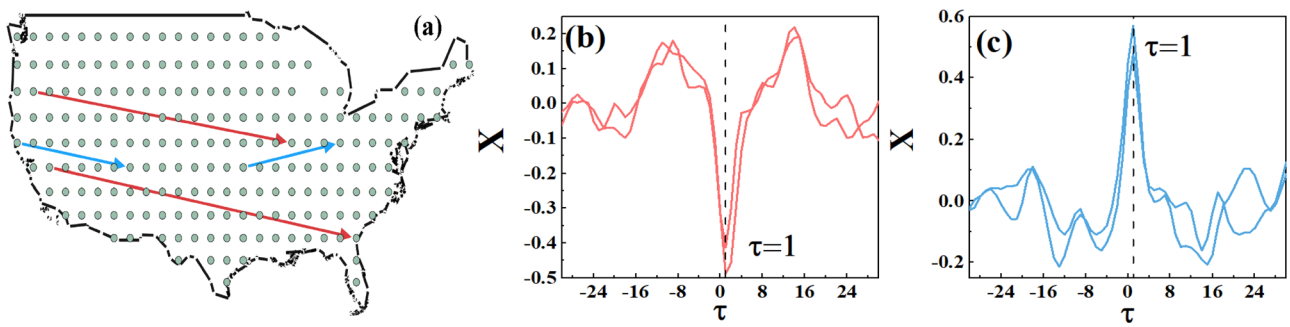

Fig. 1 | Example of establishing links of network. a An example for demonstration of four carbon flux network links based on 2017–2018 carbon flux data from the USA. Red arrows (direction of the link) represent negatively correlated links, and blue arrows represent positively correlated links. **b**, **c** Shown are the cross-correlation functions of the negative weighted links and positive weighted links (red and blue curves) for **a**, respectively.

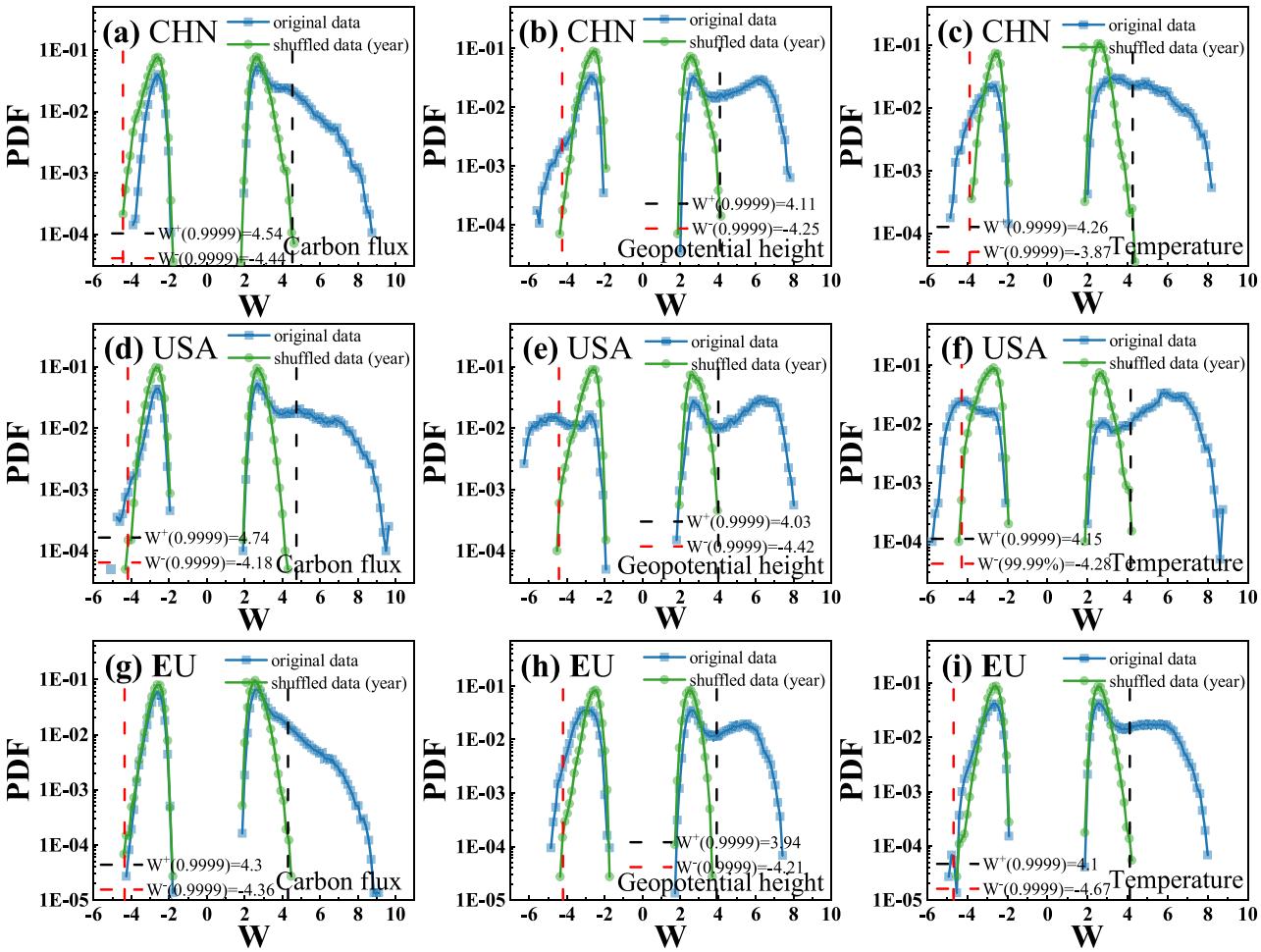

Fig. 2 | Probability distribution function (PDF) of link weights for the real-time window data and for the random shuffled data for the years 2017–2018. PDFs of link weights W of carbon flux, geopotential height, and temperature for different regions: **a**–**c** CHN, **d**–**f** USA, and **g**–**i** EU. The square points are the PDF of the link weight of the real records, the circle is the PDF of the link weight for the shuffled data, and the dashed line is the threshold of link weight above which the chance that the links obtained from the real data is less than 0.01% being random and false.

years[25,32,37]. Additionally, in Fig. 4h, one can note that during the 2013–2014 time window, the fraction of significant links differs from other years when the geographic distance exceeds 5000 km. This phenomenon can be attributed to the relatively small number of potential links within this geographic range (0.4% of total potential links), of which nearly half are significant. Consequently, the fraction of significant links in this period differs notably from that in other years.

Results

After identifying the significant links in the correlation network of climate and carbon flux constructed above (the number of significant links for each of climate and carbon flux networks for different years is given in SN2 Fig. S23), we wish to measure here the persistence (similarity) of the spatial network during the years. To this end, we analyze their temporal persistence during the recent 20 years using Jaccard similarity coefficients[38]. We focus here only on positive weighted links, since as seen in SN2 Figs. S2–S16, most networks have few negative weighted links. The Jaccard similarity is defined as the ratio between the intersection of the links in both networks in different years and the union number of links in both networks. The number of link intersections/unions for each two networks is shown in SN2 Figs. S24 and S25. Based on the definition of the Jaccard similarity coefficient, one can conclude that a higher Jaccard index in the networks indicates a greater structural similarity between the networks in these years. This, in turn, signifies a stronger persistence in the spatial and temporal evolution of the network system. Therefore, Jaccard similarity coefficients are chosen in this study to measure the structural persistence of the climate networks and of the carbon flux network. We present the actual Jaccard coefficient results in SN2 Figs. S26–S28, demonstrating significant persistence during the years in the carbon flux and climate networks. However, when the geographic distance is above 1000km, as shown in SN2 Fig. S28, it becomes evident that the links between the carbon flux and climate networks in the regions of China and Europe exhibit much less persistence. Note also that the persistence of precipitation is lower compared to climate, in particular in Europe.

In particular, to test the persistence significance, we randomly chose the same number of edges for networks i and j as in the original two different years networks and placed them between pairs of nodes chosen randomly and measure J_{ij}^{ran}. The controlled process is iterated 500 times, and the Jaccard coefficient in the controlled scenario (J^{ran}) is determined as the average value of J_{ij}^{ran} computed across these 500 iterations (see SN2 Figs. S29–S31). Next, we examined the value of the actual Jaccard coefficient (J_{ij}) with respect to the values of the Jaccard coefficient in the controlled random case (J^{ran}) for determining the significance (t-test). Note that the results for the cumulative distribution function of the actual Jaccard coefficient and Jaccard coefficient in the controlled case are shown in SN2 Figs. S32–S34. The t-test reveals that the actual Jaccard coefficients are significantly higher and different ($p < 0.05$) from the Jaccard coefficients in the controlled random case. Thus, the average of the Jaccard similarity coefficients in the controlled random case ($\overline{J^{ran}}$) is subtracted from the actual Jaccard similarity coefficients to obtain the corrected effective Jaccard

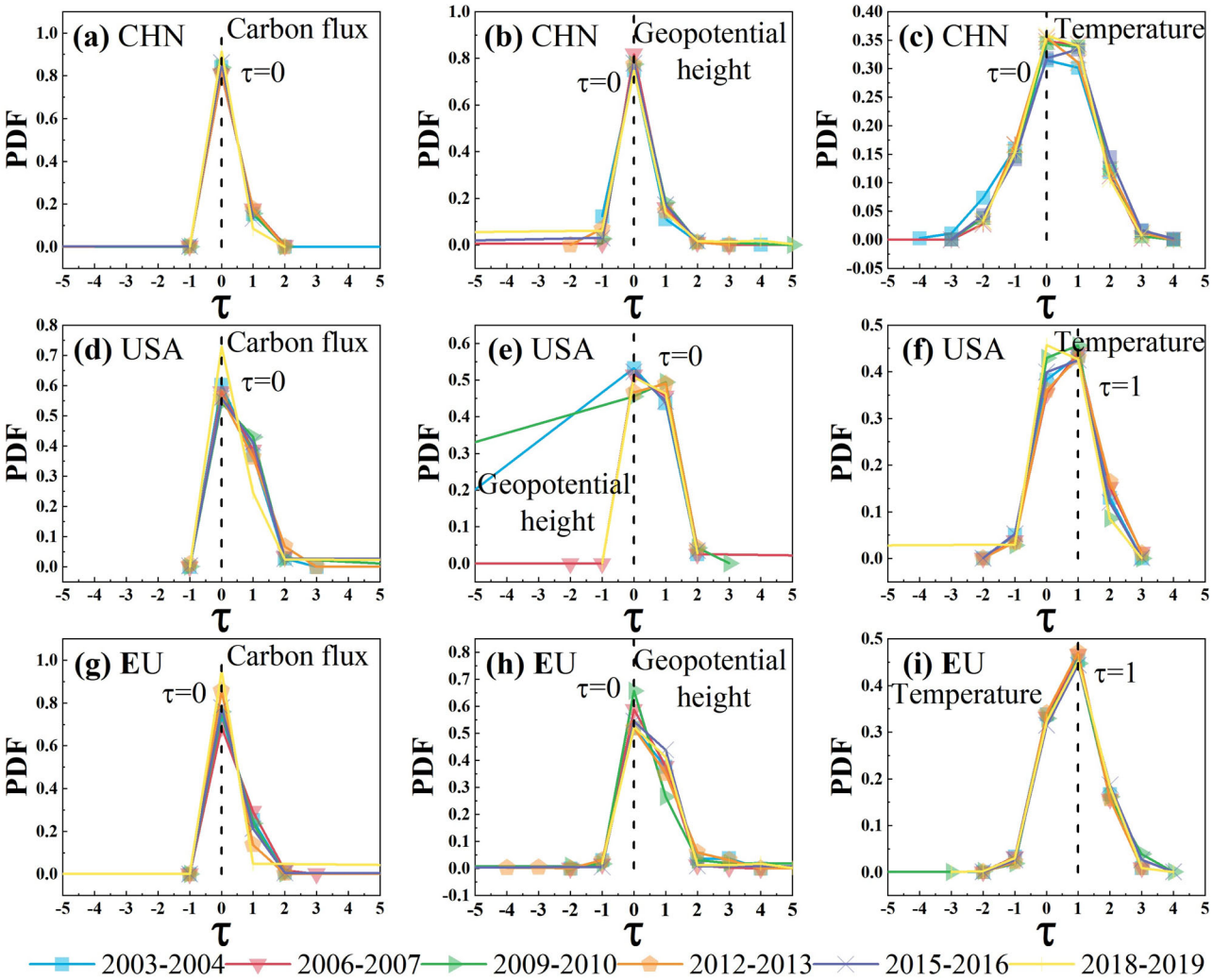

Fig. 3 | Probability distribution functions (PDF) of the time lags, τ, of the real links in different time series. PDFs of τ of carbon flux, geopotential height, and temperature for different regions: **a**–**c** CHN, **d**–**f** USA, and **g**–**i** EU. Different line patterns represent the time lag probability distribution of the network links for different years.

similarity coefficient (E-Jaccard), i.e., *E-Jaccard*$_{ij}$ defined—$J_{ij} - \overline{J^{ran}}$ (see SN2 Supplementary Table X for the average and standard deviation of the actual and controlled Jaccard similarity coefficients, $p < 0.05$). Figure 5 displays the effective Jaccard similarity coefficient matrix for all year pairs based on the carbon flux and climate network links (similar results of wind speed and precipitation, are shown in SN2 Fig. S35). One can observe that the effective Jaccard coefficients are in the range of 0.57 ± 0.07 ($p < 0.05$) for different carbon flux and climate variables in different regions. This implies that the climate variables and carbon flux studied in the Earth's climate system are generally persistent and maintain a steady state. It is notable that the similarity between a given year and the years after does not decay systematically—but only when averaged (see SN2 Fig. S41). This suggests further that there is, on average, a small decay, but the persistent network of links is quite stable. However, note that, for the carbon flux network in China, unique low values of Jaccard have been observed in two years, 2004–2005 and 2015–2016. This could be related to the fact that in 2004, China became the world's largest emitter of CO_2, although forests in the country absorbed more than 8% of national emissions during that year[39]. The following year, 2005, CO_2 emissions reached a new record high. Also, in 2015, China's carbon emissions declined for the first time, marking a turning point in the country's carbon emissions[40]. These results indicate that China has been actively pursuing the goals of the "Paris Agreement". In addition, Fig. 5b, h, the geopotential height networks in China and Europe, under the general persistence, also show unique low Jaccards in the 2008-2009 and 2007-2008 time windows, respectively. This finding can be probably attributed to the largest snow extent in Eurasia in January 2008, and the unusually warm temperatures resulted in the smallest spring snow extent in Eurasia in March and April 2008, leading to severe winter weather and unique behavior of geopotential heights in Eurasia[41,42]. Furthermore, the Jaccard similarity coefficients of the links of each two networks in carbon flux and climate variables are also analyzed for links having geographic distances above 500 km and 1000 km (see SN2 Figs. S36 and S37). For links above 500 km the Jaccard values are within the range of 0.55 ± 0.09, and for links above 1000 km the Jaccard values are within the range of 0.47 ± 0.15 ($p < 0.05$). Thus, the similarity represented by the Jaccard values decreases as the geographical distance between nodes increases. Moreover, we analyze the average of Jaccard similarity coefficients based on the effective Jaccard similarity coefficient matrix, considering between intervals ranging from one to five years (i.e., averaging over each of the first five diagonal columns below the central dark green column of Fig. 5) (see SN2 Figs. S41). One can observe, in general, a gradually decreasing trend in the average of Jaccard as the interval years increase. Note that the decrease is significant at the interval of two years, followed by a slow decreasing trend subsequently. This phenomenon can be attributed to the presence of a 365-day overlap in the data for a one-year interval, resulting in an increased similarity in the network structure, which in turn leads to a higher average of the Jaccard value. Thus, when the interval of two years, the decrease in the average value of Jaccard reaches the most significant extent. Nevertheless, one can see that the

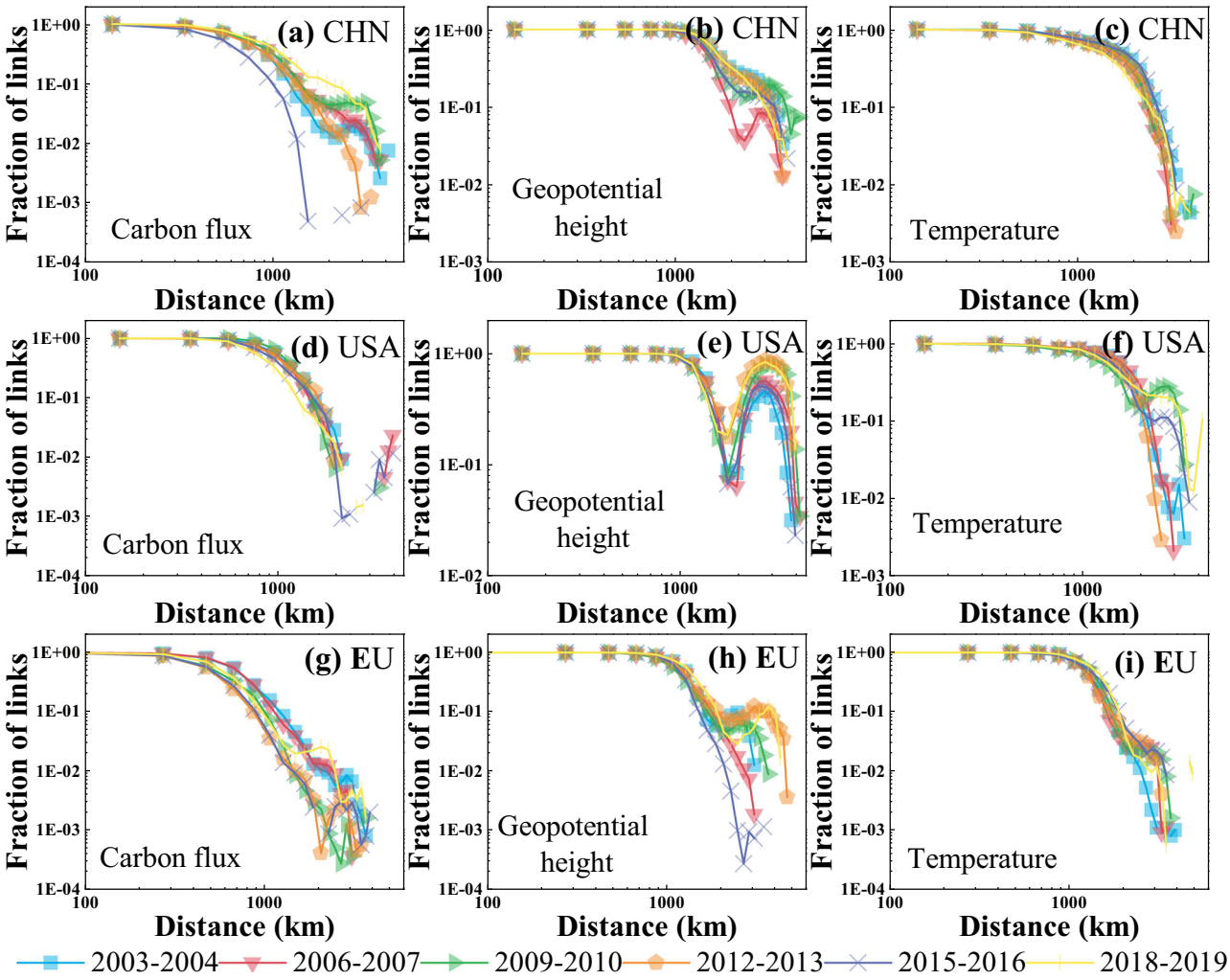

Fig. 4 | Fraction of significant links in the network as a function of geographic distance between the sites for different time series. Fraction of significant links of carbon flux, geopotential height, and temperature for different regions: **a**–**c** CHN, **d**–**f** USA, and **g**–**i** EU. Different line patterns represent the fraction of significant links as a function of geographic distance between sites of the network in different years.

similarity of the climate network slightly decreases with years, which is reflected in the gradual decrease in persistence. This decay is consistent and could be related to the decay found by Koscielny-Bunde et al.[5] in their study of the persistence of localized climate variables, where the autocorrelation of temperature in a given location decays as a power-law. The decay in ref. 5 represents the decay in the similarity of the signal of each node, while the present decay represents the decay of the global network, which is represented by links (interactions) between nodes. In addition, we notice that the trends of climatic variables in different regions at different geographic distances remain generally consistent. Notably, within the China region, there is a noteworthy slow increase in the persistence of temperature and wind speed after the interval of 3 years. This change in trend may reflect climate dynamics processes or climate variability patterns specific to China.

In addition, this paper extends the Jaccard similarity coefficient by analyzing the variation of Jaccard similarity coefficients with years within each of the two networks for different geographical distances. To test the significance of our results, we analyze the network structure shuffled at least 500 times to obtain the Jaccard similarity coefficients at different geographic distances in the controlled scenario. The findings, depicted in Fig. 6, reveal that in the controlled scenario, the Jaccard similarity coefficient at different geographic distances is consistently lower than the corresponding actual Jaccard similarity coefficient (similar results of wind speed and precipitation, are shown in SN2 Fig. S42). Furthermore, in contrast to the carbon flux network, the Jaccard index of the other climate networks exhibits similarity for the two networks at different times. It is also seen that the shorter geographical links are significantly, more similar over the years. The results are consistent with those in Fig. 4, with increasing geographic distance, the number of significant links decreases, i.e., there are fewer connections between more distant geographic distances. Moreover, the Jaccard value is also smaller, i.e., there is less climatic similarity between longer geographic distances. Furthermore, Fig. 6a, e shows some anomalies of the large number of links at geographic distances between 1500–3500 km, suggesting the potential impact of Rossby waves of half wavelength at these scales[24,32]. Finally, we statistically characterize the topological structure of the carbon flux and climate networks (see SN2 Figs. S46–S49) and observe that they obey a Poisson distribution, which indicates that most of the node degrees are close to the average degree and consistent with the high persistence of the network topology shown in Fig. 5. Furthermore, we identify communities of climate and carbon flux networks using the Louvain algorithm, and SN2 Fig. S47 shows the fluctuation of giant community sizes over time. In China, the giant community size of geopotential height is the largest and fluctuates around 110. For the United States, the giant community size of the precipitation network is the smallest. For Europe, they fluctuate around 110.

Conclusions

In this manuscript we developed a framework to study the time persistence of climate networks. While the persistence of single records such as climate,

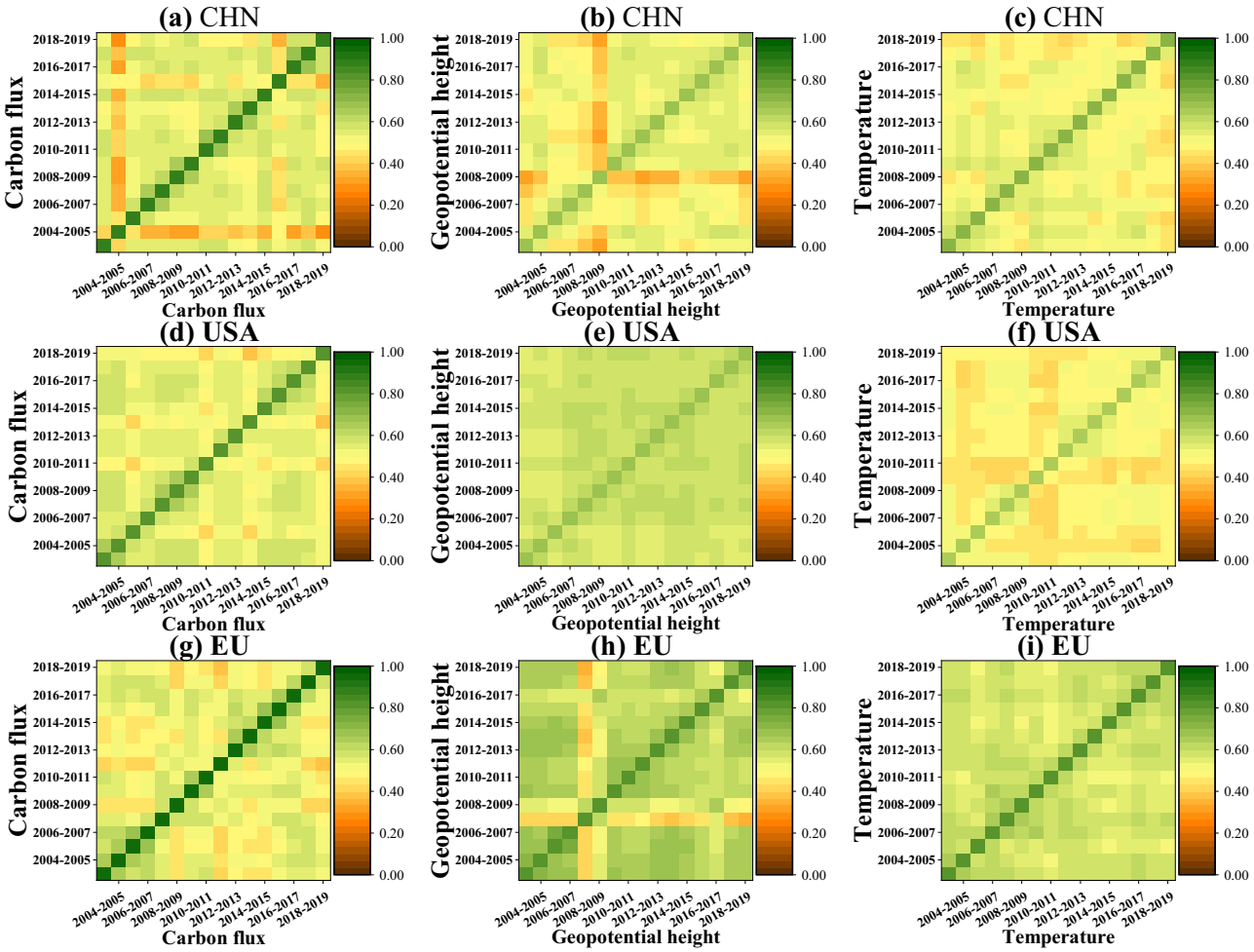

Fig. 5 | The effective Jaccard similarity coefficient matrix for links in two networks of different years for each of the climate variables. The effective Jaccard similarity coefficient matrix of carbon flux, geopotential height, and temperature for different regions: **a**–**c** CHN, **d**–**f** USA, and **g**–**i** EU. Each matrix element represents the difference between the actual Jaccard similarity coefficient and the corresponding average values obtained from the controlled random case.

heartbeat, and DNA sequences have been extensively studied[43], the persistence of a network as a whole has been rarely addressed. The steady state is a crucial feature of the climate and carbon flux system, playing an essential role in understanding climate changes in the Earth system. However, the persistence and steady state of the climate and carbon flux systems are not yet fully understood. In this study, we construct climate and carbon networks where nodes are spatial locations, and links are derived based on evaluating the cross-correlations between climate variables and carbon flux in different locations. This framework enables testing the similarity between the networks in different years in order to evaluate the persistence of the climate and carbon systems.

We investigate the similarity of climate and carbon flux networks in different years for three land regions, namely East Asia (China), North America (contiguous United States), and Europe, using daily data on climate and carbon flux during 2000–2019. We focus on the spatio-temporal perspective to explore the evolution of the similarity of the system network structure. The results indicate that the similarity of the climate and carbon flux networks between different years represented by the Jaccard measure is in the range of 0.57 ± 0.07 ($p < 0.05$). That is close to 50% of the links remain the same during the years, indicating that the correlation network structure of the system is generally persistent and in a stable state. However, the carbon flux network in China exhibits unique behavior in specific two years, 2004–2005 and 2015–2016, which is probably attributed to China's rapid development and active participation in the "Paris Agreement". On the other hand, the study reveals that the persistence of the network structure of climate and carbon flux networks tends to significantly decrease as the geographical distance increases. Finally, our developed persistence framework provides a methodology and theoretical framework for the network persistence of carbon flux and climate system network structure, which helps to explore the structural steady state of the Earth's climate system useful tool to test the quality of models, testing and predicting in good models future persistence, better understanding the impact of global warming, and provide the scientific basis and proper response to climate change. Since the current study mainly focuses on developing a framework for network persistence, we use the limited but accurate records of 20 years only, as well as the interactions within each layer only. The present study is concerned with developing the concept and the framework for persistence concept and how to measure it. Thus, we focus on the persistence of climate same variable networks rather than interactions between different variables. However, in order to better understand the effect of climate behavior, our near future study will focus on considering longer time periods and including the interactions between different climate variables as well as future data predicted by models, to deeply explore the time persistence of climate networks. We will also test the model's ability to predict climate networks and test persistence in high-quality models that predict future climate data.

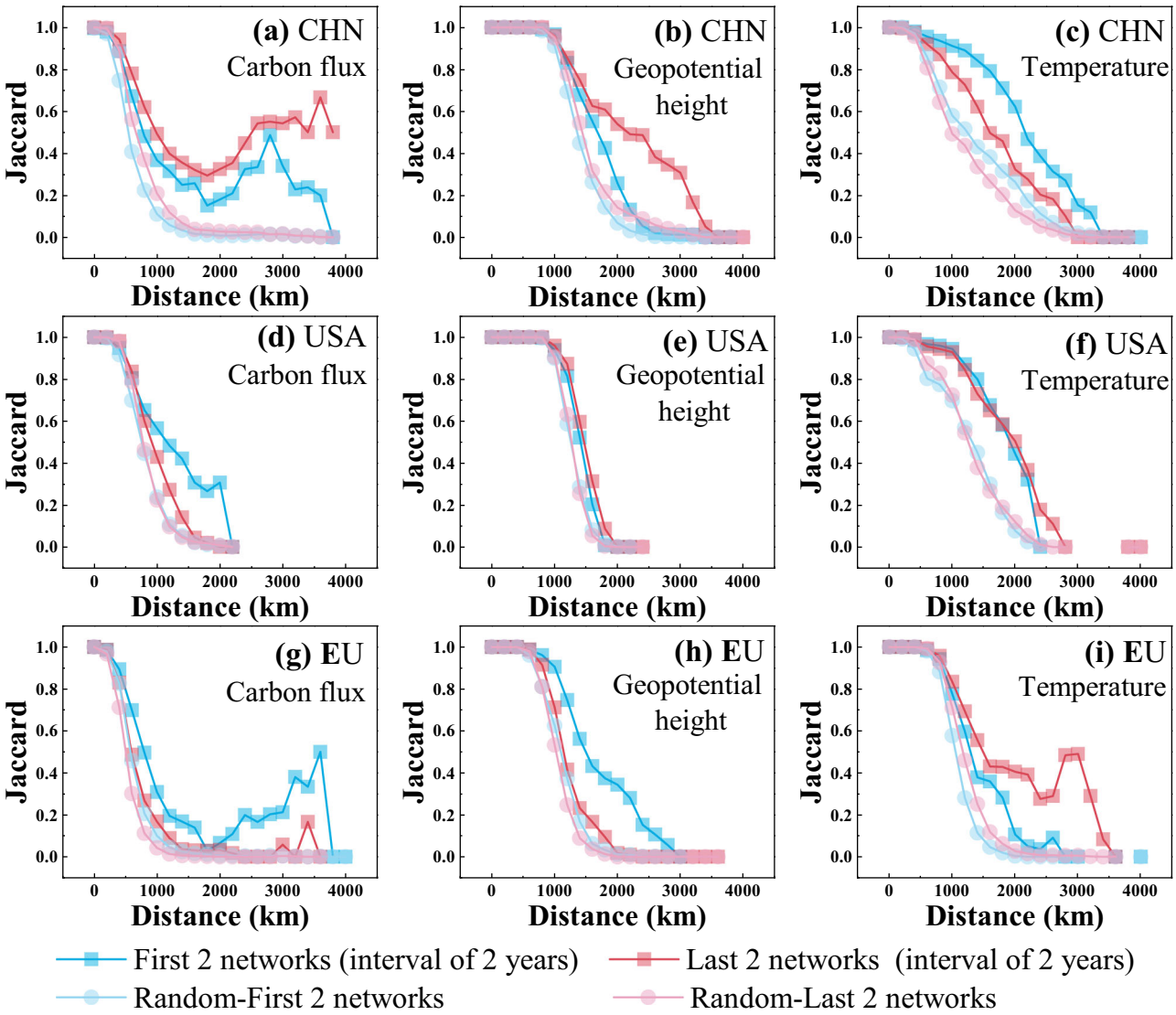

Fig. 6 | Variation of Jaccard similarity coefficients for two yearly networks at different geographical distances. The variation of carbon flux, geopotential height, and temperature for different regions: **a**–**c** CHN, **d**–**f** USA, and **g**–**i** EU. Darker colors represent the variation of Jaccard's similarity coefficients for actual scenarios. Light colors represent the variation of Jaccard's similarity coefficients for random scenarios.

Data availability

The climate variables dataset used here is publicly available at https://cds.climate.copernicus.eu/cdsapp#!/dataset/reanalysis-era5-single-levels. The carbon flux data used here is publicly available at https://gml.noaa.gov/ccgg/carbontracker/. All other data that support the plots within this paper and other findings of this study are available from the first author (Q.T.) upon reasonable request. Supplementary Data 1 is the numerical source data for graphs and charts.

Code availability

The custom codes using well-established algorithms used for the experiment analysis and numerical calculation are available from the corresponding author upon reasonable request.

Received: 19 April 2024; Accepted: 6 November 2024;
Published online: 16 November 2024

References

1. Salcedo-Sanz, S. et al. Persistence in complex systems. *Phys. Rep.* **957**, 1–73 (2022).
2. Wang, Y., Zhou, D., Bunde, A. & Havlin, S. Testing reanalysis data sets in Antarctica: trends, persistence properties, and trend significance. *J. Geophys. Res. Atmos.* **121**, 12–839 (2016).
3. Schellnhuber, H.-J. Power-law persistence and trends in the atmosphere: A detailed study of long temperature records. *Phys. Rev. E* **68**, 046133 (2003).
4. World Meteorological Organization. *WMO Greenhouse Gas Bulletin (GHG Bulletin)-No. 14: The State of Greenhouse Gases in the Atmosphere Based on Global Observations through 2017* (World Meteorological Organization, 2017).
5. Koscielny-Bunde, E. et al. Indication of a universal persistence law governing atmospheric variability. *Phys. Rev. Lett.* **81**, 729 (1998).
6. Kantelhardt, J. W. et al. Long-term persistence and multifractality of precipitation and river runoff records. *J. Geophys. Res. Atmos.* **111**, https://doi.org/10.1029/2005JD005881 (2006).
7. Hardstone, R. et al. Detrended fluctuation analysis: a scale-free view on neuronal oscillations. *Front. Physiol.* **3**, 450 (2012).
8. Panchev, S. & Tsekov, M. Empirical evidences of persistence and dynamical chaos in solar–terrestrial phenomena. *J. Atmos. Sol. Terrest. Phys.* **69**, 2391–2404 (2007).

9. Bunde, A. & Havlin, S. Power-law persistence in the atmosphere and in the oceans. *Phys. A: Stat. Mech. Appl.* **314**, 15–24 (2002).
10. Wunderling, N. et al. Global warming overshoots increase risks of climate tipping cascades in a network model. *Nat. Clim. Change* **13**, 75–82 (2023).
11. Liu, T. et al. Teleconnections among tipping elements in the Earth system. *Nat. Clim. Change* **13**, 67–74 (2023).
12. Bulgin, C. E., Merchant, C. J. & Ferreira, D. Tendencies, variability and persistence of sea surface temperature anomalies. *Sci. Rep.* **10**, 7986 (2020).
13. Rousi, E., Kornhuber, K., Beobide-Arsuaga, G., Luo, F. & Coumou, D. Accelerated western European heatwave trends linked to more-persistent double jets over Eurasia. *Nat. Commun.* **13**, 3851 (2022).
14. Koçak, K. Practical ways of evaluating wind speed persistence. *Energy* **33**, 65–70 (2008).
15. Dai, X., Wang, P., Zhang, P. & Chou, J. Rainfall spectrum change in North China and its possible mechanism. *Prog. Nat. Sci.* **14**, 598–604 (2004).
16. Ludescher, J. et al. Network-based forecasting of climate phenomena. *Proc. Natl Acad. Sci. USA* **118**, e1922872118 (2021).
17. Yamasaki, K., Gozolchiani, A. & Havlin, S. Climate networks around the globe are significantly affected by El Niño. *Phys. Rev. Lett.* **100**, 228501 (2008).
18. Banerjee, A. et al. Spatial coherence patterns of extreme winter precipitation in the US. *Theoret. Appl. Climatol.*, **152**, 385–395 (2023).
19. Sunny, E. M., Balakrishnan, J. & Kurths, J. Predicting climatic tipping points. *Chaos Interdiscip. J. Nonlinear Sci.* **33**, 021101 (2023).
20. Lu, Z. et al. Early warning of the Indian Ocean Dipole using climate network analysis. *Proc. Natl Acad. Sci. USA* **119**, e2109089119 (2022).
21. Fan, J., Meng, J., Ashkenazy, Y., Havlin, S. & Schellnhuber, H. J. Climate network percolation reveals the expansion and weakening of the tropical component under global warming. *Proc. Natl Acad. Sci. USA* **115**, E12128–E12134 (2018).
22. Ludescher, J. et al. Improved El Niño forecasting by cooperativity detection. *Proc. Natl Acad. Sci.* **110**, 11742–11745 (2013).
23. Zhou, D., Gozolchiani, A., Ashkenazy, Y. & Havlin, S. Teleconnection paths via climate network direct link detection. *Phys. Rev. Lett.* **115**, 268501 (2015).
24. Zhang, Y., Fan, J., Chen, X., Ashkenazy, Y. & Havlin, S. Significant impact of Rossby waves on air pollution detected by network analysis. *Geophys. Res. Lett.* **46**, 12476–12485 (2019).
25. Wang, Y. et al. Dominant imprint of Rossby waves in the climate network. *Phys. Rev. Lett.* **111**, 138501 (2013).
26. Pachauri, R. K. et al. *Climate Change 2014: Synthesis Report. Contribution of Working Groups I, II and III to the Fifth Assessment Report of the Intergovernmental Panel on Climate Change* (IPCC, 2014).
27. Hersbach, H. et al. *ERA5 Hourly Data on Pressure Levels From 1959 to Present*. (Copernicus Climate Change Service (C3S) Climate Data Store (CDS), (2018). Accessed on May 1, 2020.
28. Jacobson, A. R., Schuldt, K. N. & Miller, E. A. CarbonTracker CT2019B (2020). https://www.esrl.noaa.gov/gmd/ccgg/carbontracker/CT2019B/
29. Leung, D. M. et al. Synoptic meteorological modes of variability for fine particulate matter (PM 2.5) air quality in major metropolitan regions of China. *Atmos. Chem. Phys.* **18**, 6733–6748 (2018).
30. Tai, A. P., Mickley, L. J. & Jacob, D. J. Correlations between fine particulate matter (PM 2.5) and meteorological variables in the United States: Implications for the sensitivity of PM 2.5 to climate change. *Atmos. Environ.* **44**, 3976–3984 (2010).
31. Wang, M., Tian, L. & Du, R. Research on the interaction patterns among the global crude oil import dependency countries: a complex network approach. *Appl. Energy* **180**, 779–791 (2016).
32. Ying, N. et al. Rossby waves detection in the CO_2 and temperature multilayer climate network. *Geophys. Res. Lett.* **47**, e2019GL086507 (2020).
33. Gozolchiani, A., Yamasaki, K., Gazit, O. & Havlin, S. Pattern of climate network blinking links follows El Niño events. *EPL (Europhys. Lett.)* **83**, 28005 (2008).
34. Guez, O. C., Gozolchiani, A. & Havlin, S. Influence of autocorrelation on the topology of the climate network. *Phys. Rev. E* **90**, 062814 (2014).
35. Du, R. et al. Identifying the peak point of systemic risk in international crude oil importing trade. *Energy* **176**, 281–291 (2019).
36. Fan, J., Meng, J., Ashkenazy, Y., Havlin, S. & Schellnhuber, H. J. Network analysis reveals strongly localized impacts of El Niño. *Proc. Natl Acad. Sci. USA* **114**, 7543–7548 (2017).
37. Riboldi, J., Rousi, E., d'Andrea, F., Rivière, G. & Lott, F. Circumglobal Rossby wave patterns during boreal winter highlighted by space–time spectral analysis. *Weather Clim. Dyn.* **3**, 449–469 (2022).
38. Real, R. & Vargas, J. M. The probabilistic basis of Jaccard's index of similarity. *Syst. Biol.* **45**, 380–385 (1996).
39. Washington, D. W. R. I. *Climate Watch Historical GHG Emissions (1990-2020)* (2023). https://www.climatewatchdata.org/ghg-emissions
40. Development, N. & of China (NDRC), R. C. *Enhanced Actions on Climate Change: China's Intended Nationally Determined Contributions* (2023). http://www.ndrc.gov.cn/gzdt/201506/t20150630_710226.html
41. World Meteorological Organization. *WMO Statement on the State of the Global Climate in 2008* (World Meteorological Organization, 2009).
42. Fink, A. H., Brücher, T., Ermert, V., Krüger, A. & Pinto, J. G. The European storm Kyrill in January 2007: synoptic evolution, meteorological impacts and some considerations with respect to climate change. *Nat. Hazards Earth Syst. Sci.* **9**, 405–423 (2009).
43. Buldyrev, S. et al. *in Fractals in Science*. (eds Bunde, A. & Havlin, S.) chap. 4 (Springer, 2013).

Acknowledgements

This research is supported by grants from the National Key Research and Development Program of the Ministry of Science and Technology of China (Grant No. 2020YFA0608601), National Natural Science Foundation of China (Grant No. 72174091, 62373169), Major Projects of the National Social Science Foundation of China (Grant No. 22&ZD136), Science and technology innovation project of Carbon Peaking and Carbon Neutrality of Jiangsu Province of China (Grant No. BE2022612), National Statistical Science Research Project (Grant No. 2022LZ03), Special Project of Emergency Management Institute of Jiangsu University (Grant No. KY-A-08), Israel Science Foundation (Grant No. 189/19), Binational Israel-China Science Foundation (Grant No. 3132/19), Science Minister-Smart Mobility (Grant No. 1001706769), European Union's Horizon 534 2020 research and innovation program (DIT4Tram, Grant Agreement 953783), and the Jiangsu Postgraduate Research and Innovation Plan (Grant No. KYCX22_3662). Ting Qing acknowledges the support from the program of the China Scholarship Council.

Author contributions

G.D., L.T., and S.H. designed the research, conceived the study, carried out the analysis, and prepared the manuscript. T.Q., F.W., and Q.L. performed the numerical calculations and drafted the manuscript. T.Q., F.W., Q.L., G.D., L.T., and S.H. discussed the results and revised and improved the manuscript. G.D. and S.H. led the writing of the manuscript.

Competing interests

The authors declare no competing interests.

Additional information

Supplementary information The online version contains supplementary material available at https://doi.org/10.1038/s42005-024-01862-9.

Correspondence and requests for materials should be addressed to Gaogao Dong, Lixin Tian or Shlomo Havlin.

Peer review information *Communications Physics* thanks Abhirup Banerjee and the other, anonymous, reviewer(s) for their contribution to the peer review of this work.